Chapter 7

Image Fusion Based on Shearlets

Miao Qiguang, Shi Cheng and Li Weisheng

Additional information is available at the end of the chapter

http://dx.doi.org/10.5772/56945

1. Introduction

Image decomposition is important to image fusion and affects the information extraction quality, even the whole fusion quality. Wavelet theory has been developed since the beginning of the last century. It was first applied to signal processing in the 1980's[1], and over the past decade it has been recognized as having great potential in image processing applications, as well as in image fusion[2]. Wavelet transforms are more useful than Fourier transforms, and it is efficient in dealing with one-dimensional point-wise smooth signal [3-5]. However the limitations of the direction make it not perform well for multidimensional data. Images contain sharp transition such as edges, and wavelet transforms are not optimally efficient in representing them.

Recently, a theory for multidimensional data called multi-scale geometric analysis (MGA) has been developed. Many MGA tools were proposed, such as ridgelet, curvelet, bandelet, contourlet, etc [6-9]. The new MGA tools provide higher directional sensitivity than wavelets. Shearlets, a new approach provided in 2005, possess not only all above properties, but equipped with a rich mathematical structure similar to wavelets, which are associated to a multiresolution analysis. The shearlets form a tight frame at various scales and directions, and are optimally sparse in representing images with edges. Only the curvelets has the similar properties with shearlets [10-14]. But the construction of curvelets is not built directly in the discrete domain and it does not provide a multiresolution representation of the geometry. The decomposition of shearlets is similar to contourlets, while the contourlet transform consists of an application of the Laplacian pyramid followed by directional filtering, for shearlets, the directional filtering is replaced by a shear matrix. An important advantage of the shearlet transform over the contourlet transform is that there are no restrictions on the direction numbers. [15-19]

In recent years, the theory of the shearlets, which is used in image processing, has been studied gradually. Now the applications of shearlets are mainly in image denoising, sparse image representation [20] and edge detection [21, 22]. Its applications in image fusion are still under exploring.

2. Shearlets [12, 20]

2.1. The theory of Shearlets

In dimension $n=2$, the affine systems with composite dilations are defined as follows.

$$A_{AS}(\psi)=\{\psi_{j,l,k}(x)=|\det A|^{j/2}\,\psi(S^{l}A^{j}x-k):j,l\in\mathbb{Z},k\in\mathbb{Z}^{2}\} \tag{1}$$

Where $\psi\in L^{2}(\mathbb{R}^2)$, A, S are both 2×2 invertible matrices, and $|\det S|=1$, the elements of this system are called composite wavelet if $A_{AS}(\psi)$ forms a tight frame for $L^{2}(\mathbb{R}^2)$.

$$\sum_{j,l,k}|<f,\psi_{j,l,k}>|^{2}=\|f\|^{2}$$

Let A denote the parabolic scaling matrix and S denote the shear matrix. For each $a>0$ and $s\in\mathbb{R}$,

$$A=\begin{pmatrix}a & 0\\ 0 & \sqrt{a}\end{pmatrix},S=\begin{pmatrix}1 & s\\ 0 & 1\end{pmatrix}.$$

The matrices described above have the special roles in shearlet transform. The first matrix $\begin{pmatrix}a & 0\\ 0 & \sqrt{a}\end{pmatrix}$ controls the 'scale' of the shearlets, by applying a fine dilation faction along the two axes, which ensures that the frequency support of the shearlets becomes increasingly elongated at finer scales. The second matrix $\begin{pmatrix}1 & s\\ 0 & 1\end{pmatrix}$, on the other hand, is not expansive, and only controls the orientation of the shearlets. The size of frequency support of the shearlets is illustrated in Fig. 1 for some particular values of a and s.

$\psi_{j,l,k}$ for different values of a and s.

In references [12], assume $a=4$, $s=1$, where $A=A_0$ is the anisotropic dilation matrix and $S=S_0$ is the shear matrix, which are given by

$$A_0=\begin{pmatrix}4 & 0\\ 0 & 2\end{pmatrix},\qquad S_0=\begin{pmatrix}1 & 1\\ 0 & 1\end{pmatrix}$$

For $\forall\,\xi=(\xi_1,\xi_2)\in\hat{\mathbb{R}}^2$, $\xi_1\neq0$, let $\hat{\psi}^{(0)}(\xi)$ be given by

http://dx.doi.org/10.5772/56945

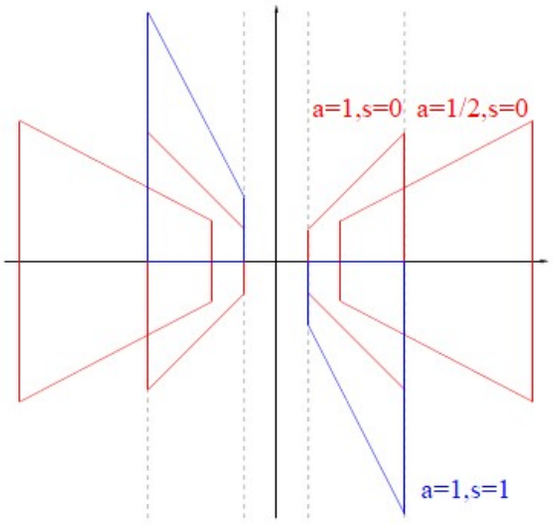

Figure 1. frequency support of the shearlets

$$\hat{\psi}^{(0)}(\xi) = \hat{\psi}^{(0)}(\xi_1, \xi_2) = \hat{\psi}_1(\xi_1)\hat{\psi}_2(\frac{\xi_2}{\xi_1}) \tag{2}$$

Where $\hat{\psi}_1 \in C^\infty(\mathbb{R})$ is a wavelet, and $\text{supp}\hat{\psi}_1 \subset [-1/2, -1/16] \cup [1/16, 1/2]$; $\hat{\psi}_2 \in C^\infty(\mathbb{R})$, and $\text{supp}\hat{\psi}_2 \subset [-1,1]$. This implies $\hat{\psi}^{(0)} \in C^\infty(\mathbb{R})$, and $\text{supp}\hat{\psi}^{(0)} \subset [-1/2, 1/2]^2$.

In addition, we assume that

$$\sum_{j\geq 0} |\hat{\psi}_1(2^{-2j}\omega)|^2 = 1, \qquad |\omega| \geq 1/8 \tag{3}$$

and for $\forall\ j \geq 0$

$$\sum_{l=-2^j}^{2^j-1} |\hat{\psi}_2(2^j\omega - l)|^2 = 1, \qquad |\omega| \leq 1 \tag{4}$$

There are several examples of functions ψ_1, ψ_2 satisfying the properties described above. Eq. (3) and (4) imply that

$$\sum_{j\geq 0}\sum_{l=-2^j}^{2^j-1} |\hat{\psi}^{(0)}(\xi A_0^{-j} S_0^{-l})|^2 = \sum_{j\geq 0}\sum_{l=-2^j}^{2^j-1} |\hat{\psi}_1(2^{-2j}\xi_1)|^2 |\hat{\psi}_2(2^j \frac{\xi_2}{\xi_1} - l)|^2 = 1, \tag{5}$$

for any $(\xi_1, \xi_2) \in D_0$, where $D_0 = \{(\xi_1, \xi_2) \in \hat{\mathbb{R}}^2 : |\xi_1| \geq 1/8, |\xi_2| \leq 1\}$, the functions $\{\hat{\psi}^{(0)}(\xi A_0^{-j} S_0^{-l})\}$ form a tiling of D_0. This is illustrated in Fig.2 (a). This property described above implies that the collection

$$\{\psi_{j,l,k}^{(0)}(x) = 2^{\frac{3j}{2}} \psi^{(0)}(S_0^l A_0^j x - k) : j \geq 0, -2^j \leq l \leq 2^j - 1, k \in \mathbb{Z}^2\} \tag{6}$$

is a Parseval frame for $L^2(D_0)^\vee = \{f \in L^2(\mathbb{R}^2) : \text{supp } \hat{f} \subset D_0\}$. And from the conditions on the support of $\hat{\psi}_1$ and $\hat{\psi}_2$ one can easily observe that the function $\psi_{j,l,k}$ have frequency support,

$$\text{supp}\, \hat{\psi}_{j,k,l}^{(0)} \subset \{(\xi_1, \xi_2) : \xi_1 \in [-2^{2j-1}, -2^{2j-4}] \cup [2^{2j-4}, 2^{2j-1}], |\frac{\xi_2}{\xi_1} + l2^{-j}| \leq 2^{-j}\} \tag{7}$$

That is, each element $\hat{\psi}_{j,l,k}$ is support on a pair of trapezoids, of approximate size $2^{2j} \times 2^j$, oriented along lines of slope $l2^{-j}$.(see Fig.2 (b)).

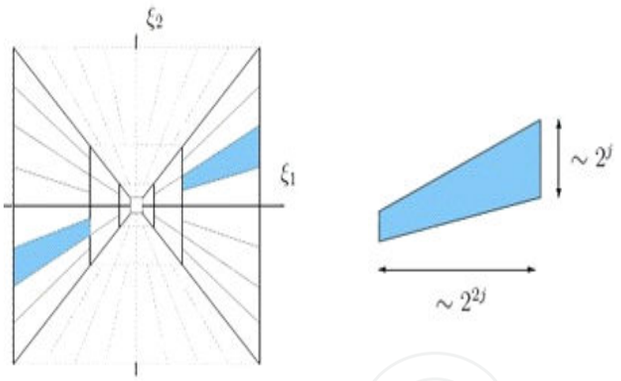

Figure 2. (a) The tiling of the frequency by the shearlets; (b) The size of the frequency support of a shearlet $\psi_{j,l,k}$.

Similarly we can construct a Parseval frame for $L^2(D_1)^\vee$, where D_1 is the vertical cone,

$$D_1 = \{(\xi_1, \xi_2) \in \hat{\mathbb{R}}^2 : |\xi_2| \geq 1/8, |\frac{\xi_1}{\xi_2}| \leq 1\}, \tag{8}$$

Let

$$A_1 = \begin{pmatrix} 2 & 0 \\ 0 & 4 \end{pmatrix}, \qquad S_1 = \begin{pmatrix} 1 & 0 \\ 1 & 1 \end{pmatrix}$$

http://dx.doi.org/10.5772/56945

and $\hat{\psi}^{(1)}(\xi)=\hat{\psi}^{(1)}(\xi_1, \xi_2)=\hat{\psi}_1(\xi_2)\hat{\psi}_2(\frac{\xi_1}{\xi_2})$, where $\hat{\psi}_1$ and $\hat{\psi}_2$ are defined as (2) and (3), then the Parseval frame for $L^2(D_1)^\vee$ is as follows,

$$\{\psi_{j,l,k}^{(1)}(x)=2^{\frac{3j}{2}}\psi^{(1)}(S_1^l A_1^j x-k): j\geq 0, -2^j\leq l\leq 2^j-1, k\in \mathbb{Z}^2\}. \tag{9}$$

To make this discussion more rigorous, it will be useful to examine this problem from the point of view of approximation theory. If $F=\{\psi_\mu : \mu\in I\}$ is a basis or, more generally, a tight frame for $L^2(R^2)$, then an image f can be approximated by the partial sums

$$f_M=\sum_{\mu\in I_M}<f,\psi_\mu>\psi_\mu, \tag{10}$$

Where I_M is the index set of the M largest inner products $|<f, \psi_\mu>|$. The resulting approximation error is

$$\varepsilon_M=\| f-f_M\|^2=\sum_{\mu\notin I_M}|f,\psi_\mu|^2, \tag{11}$$

and this quantity approaches asymptotically zero as M increases.

The approximation error of Fourier approximations is $\varepsilon_M\leq CM^{-1/2}$, of the Wavelet is $\varepsilon_M\leq CM^{-1}$, and the approximation error of Shearlets is $\varepsilon_M\leq C(\log M)^3M^{-2}$, which is better than Fourier and Wavelet approximations.

2.2. Discrete Shearlets

It will be convenient to describe the collection of shearlets presented above in a way which is more suitable to derive numerical implementation. For $\xi=(\xi_1, \xi_2)\in\hat{R}^2$, $j\geq 0$ and $l=-2^j, \cdots, 2^j-1$, Let

$$W_{j,l}^0(\xi)=\begin{cases}\hat{\psi}_2(2^j\frac{\xi_2}{\xi_1}-l)\chi_{D_0}(\xi)+\hat{\psi}_2(2^j\frac{\xi_1}{\xi_2}-l+1)\chi_{D_1}(\xi) & l=-2^j\\ \hat{\psi}_2(2^j\frac{\xi_2}{\xi_1}-l)\chi_{D_0}(\xi)+\hat{\psi}_2(2^j\frac{\xi_1}{\xi_2}-l\text{-}1)\chi_{D_1}(\xi) & l=2^j-1\\ \hat{\psi}_2(2^j\frac{\xi_2}{\xi_1}-l) & otherwise\end{cases} \tag{12}$$

and

$$W_{j,l}^{1}(\xi)=\begin{cases}\hat{\psi}_2(2^j\frac{\xi_2}{\xi_1}-l+1)\chi_{D_0}(\xi)+\hat{\psi}_2(2^j\frac{\xi_1}{\xi_2}-l)\chi_{D_1}(\xi) & l=-2^j\\ \hat{\psi}_2(2^j\frac{\xi_2}{\xi_1}-l-1)\chi_{D_0}(\xi)+\hat{\psi}_2(2^j\frac{\xi_1}{\xi_2}-l)\chi_{D_1}(\xi) & l=2^j-1\\ \hat{\psi}_2(2^j\frac{\xi_1}{\xi_2}-l) & otherwise\end{cases} \tag{13}$$

Where ψ_2, D_0, D_1 are defined in section 2. For $-2^j\le l\le 2^j-2$, each term $W_{j,l}^{(d)}(\xi)$ is a window function localized on a pair of trapezoids, as illustrated in fig.1a. When $l=-2^j$ or $l=2^j-1$, at the junction of the horizontal cone D_0 and the vertical cone, $W_{j,l}^{(d)}(\xi)$ is the superposition of two such function.

Using this notation, for $j\ge 0$, $-2^j+1\le l\le 2^j-2$, $k\in Z^2$, $d=0, 1$, we can write the Fourier transform of the Shearlets in the compact form

$$\hat{\psi}_{j,l,k}^{(d)}(\xi)=2^{\frac{3j}{2}}V(2^{-2j}\xi)W_{j,l}^{(d)}(\xi)e^{-2\pi i\xi A_d^{-j}B_d^{-l}k} \tag{14}$$

Where $V(\xi_1, \xi_2)=\hat{\psi}_1(\xi_1)\chi_{D_0}(\xi_1, \xi_2)+\hat{\psi}_1(\xi_2)\chi_{D_1}(\xi_1, \xi_2)$.

The Shearlet transform of $f\in L^2(R^2)$ can be computed by

$$<f,\psi_{j,l,k}^{(d)}>=2^{\frac{3j}{2}}\int_{R^2}\hat{f}(\xi)\overline{V(2^{-2j}\xi)W_{j,l}^{(d)}(\xi)}e^{-2\pi i\xi A_d^{-j}B_d^{-l}k}d\xi \tag{15}$$

Indeed, one can easily verify that

$$\sum_{d=0}^{1}\sum_{l=-2^j}^{2^j-1}|W_{j,l}^{(d)}(\xi_1,\xi_2)|^2=1 \tag{16}$$

And form this it follows that

$$|\hat{\phi}(\xi_1,\xi_2)|^2+\sum_{d=0}^{1}\sum_{j\ge 0}\sum_{l=-2^j}^{2^j-1}|V(2^{2j}\xi_1,2^{2j}\xi_2)||W_{j,l}^{(d)}(\xi_1,\xi_2)|^2=1 \tag{17}$$

http://dx.doi.org/10.5772/56945

3. Multi-focus image fusion based on Shearlets

3.1. Algorithm framework of multi-focus image fusion using Shearlets

3.1.1. Image decomposition

Image decomposition based on shearlet transform is composed by two parts, decomposition of multi-direction and multi-scale.

1. Multi-direction decomposition of image using shear matrix S_0 or S_1.
2. Multi-scale decompose of each direction using wavelet packets decomposition.

In step (1), if the image is decomposed only by S_0, or by S_1, the number of the directions is $2(l+1)+1$. If the image is decomposed both by S_0 and S_1, the number of the directions is $2(l+2)+2$. The framework of Image decomposition with shearlets is shown in Fig. 3.

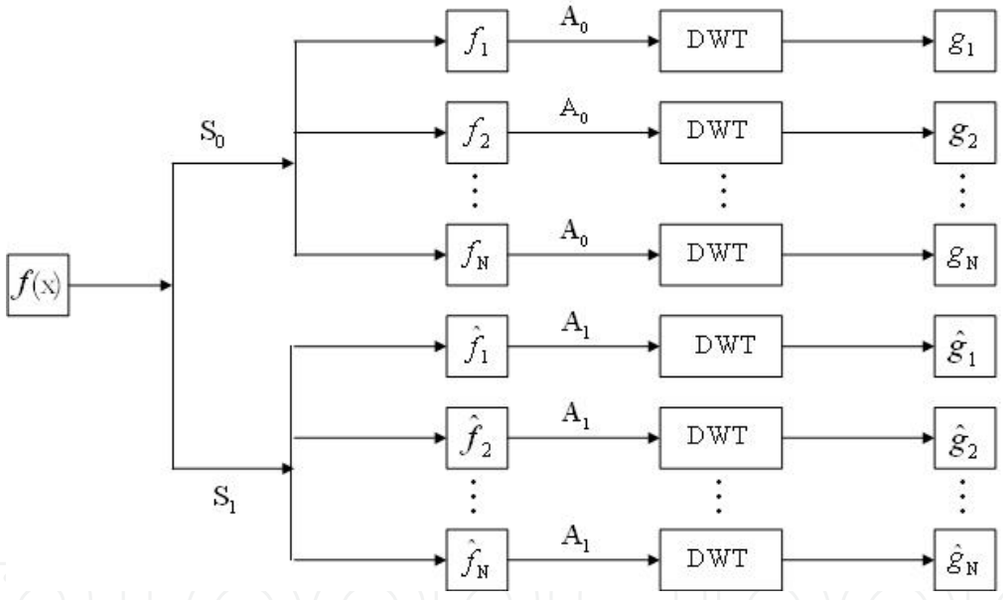

Figure 3. Image decomposition framework with shearlets

3.1.2. Image fusion

Image fusion framework based on shearlets is shown in Fig. 4. The following steps of image fusion are adopted.

1. The two images taking part in the fusion are geometrically reg is tered to each other.
2. Transform the original images using shearlets. Both horizontal and vertical cones are adopted in this method. The number of the directions is 6. Then the wavelet packets are used in multi-scale decomposition with $j=5$.

3. Fusion rule based on regional absolute value is adopted in this algorithem.

a. The choice of low frequency coefficients.

Low frequency coefficients of the fused image are replaced by the average of low frequency coefficients of the two source images.

b. The choice of high frequency coefficients.

$$D_X(i,j) = \sum_{i \le M, j \le N} |Y_X(i,j)|, \quad X = A, B \tag{18}$$

Calculate the absolute value of high frequency coefficients in the neighborhood by Eq.(18) Where $M = N = 3$ is the size of the neighborhood, X denotes the two source images, $D_X(i, j)$ is the regional absolute value of X image within 3 neighborhood with the center at (i, j), $Y_X(i, j)$ means the pixel value at (i, j) from X.

Select the high frequency coefficients from the two source images.

$$F(i,j) = \begin{cases} A(i,j) & D_A(i,j) \ge D_B(i,j) \\ B(i,j) & D_A(i,j) < D_B(i,j) \end{cases} \tag{19}$$

Where F is the high frequency coefficients of the fused image.

Finally the region consistency check is done based on the fuse-decision map, which is shown in Eq.(20).

$$Map(i,j) = \begin{cases} 1 & D_A(i,j) \ge D_B(i,j) \\ 0 & D_A(i,j) < D_B(i,j) \end{cases} \tag{20}$$

According to Eq.(20), if the certain coefficient in the fused image is to come from source image *A*, but with the majority of its surrounding neighbors from *B*, this coefficient will be switched to come from *B*.

4. The fused image is gotten using the inverse shearlet transform.

3.2. Simulation experiments

1. Multi-focus image of Bottle

The following group images are selected to prove the validity proposed in this section.

The two source images, Fig.5.(a) and (b), are the multi-focus images, which focus on the different parts. The fusion methods of these experiments are shearlets, contourlets, Haar, Daubechies, PCA and Laplacian Pyramid (LP). Fusion rule mentioned above is used in this

http://dx.doi.org/10.5772/56945

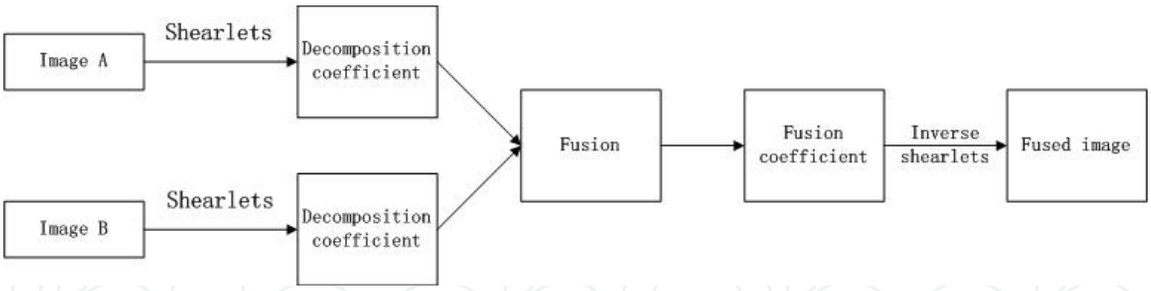

Figure 4. Image fusion framework based on shearlets

experiment. The following image quality metrics are used in this experiment: Standard deviation (STD), Difference of entropy (DEN), Overall cross entropy (OCE), Entropy (EN), Sharpness (SP), Peak signal to noise ratio (PSNR), Mean square error (MSE) and Q.

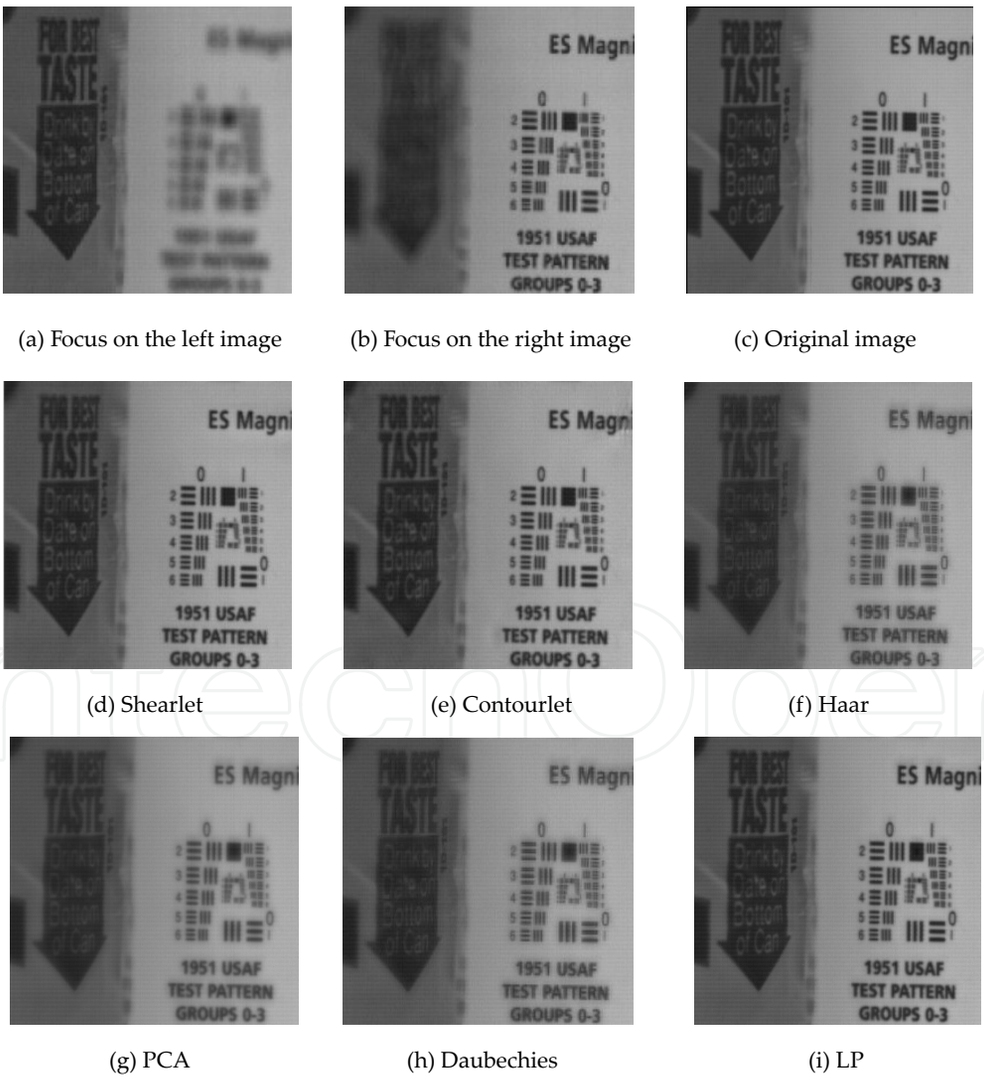

(a) Focus on the left image (b) Focus on the right image (c) Original image

(d) Shearlet (e) Contourlet (f) Haar

(g) PCA (h) Daubechies (i) LP

Figure 5. Fusion results on experiment images

Fig.5. (c) is the ideal image, Fig.5.(d) ~Fig.5.(i) are the fused images with different methods. From the subjective evaluation of Fig.6 and objective metrics from Table 1, we can see that shearlet transform have more detail information, disperse the gray level and higher sharpness of the fused image than other methods do.

	shearlet	contourlet	Haar	Daubechies	PCA	LP
STD	43.3322	43.3313	41.3589	41.2225	41.3253	44.1356
DEN	0.0021	0.0227	0.0150	0.0144	0.0113	0.0354
OCE	0.0107	0.0125	0.0442	0.0470	0.0484	0.0179
EN	6.9628	6.9577	6.9499	6.9493	6.9462	6.9703
SP	19.1502	18.7049	15.3007	14.8401	12.9532	19.4853
PSNR	40.8004	39.3935	31.4881	31.188	31.1887	40.3666
MSE	5.0067	7.0625	45.8016	49.0528	49.4549	5.9761
Q	0.9042	0.8703	0.8954	0.9010	0.9131	0.8809

Table 1. Comparison of multi-focus image fusion

2. Multi-focus Images of CT and MRI

The source images are the CT (Computer Tomography) and MRI (Magnetic Resonance Imaging) images. And Entropy (EN), Sharpness (SP), Standard deviation (STD) and Q is used to evaluate the effect of the fused images.

Fig.6 (a) is a CT image, whose brightness has relation with tissue density and the bone is shown clearly, but soft tissue is invisible. Fig.6 (b) is a MRI image, whose brightness has relation with the number of hydrogen atoms in t issue, so the soft t issue is shown clearly, but the bone is invisible. The CT image and the MRI image are complementary, the advantages could be fused into one image. The desired standard image cannot be acquired, thus only entropy and sharpness are adopted to evaluate the fusion result. Fusion rule mentioned above is used in this experiment.

	Shearlet	Contourlet	Haar	Daubechies	PCA	Average
EN	6.1851	5.9189	5.9870	5.9784	5.8792	5.9868
SP	20.5271	24.8884	16.9938	14.8810	17.2292	16.9935
STD	45.0704	50.4706	35.8754	35.1490	45.3889	34.9141
Q	0.6881	0.3022	0.4960	0.4994	0.6847	0.4943

Table 2. Comparison of medical image fusion

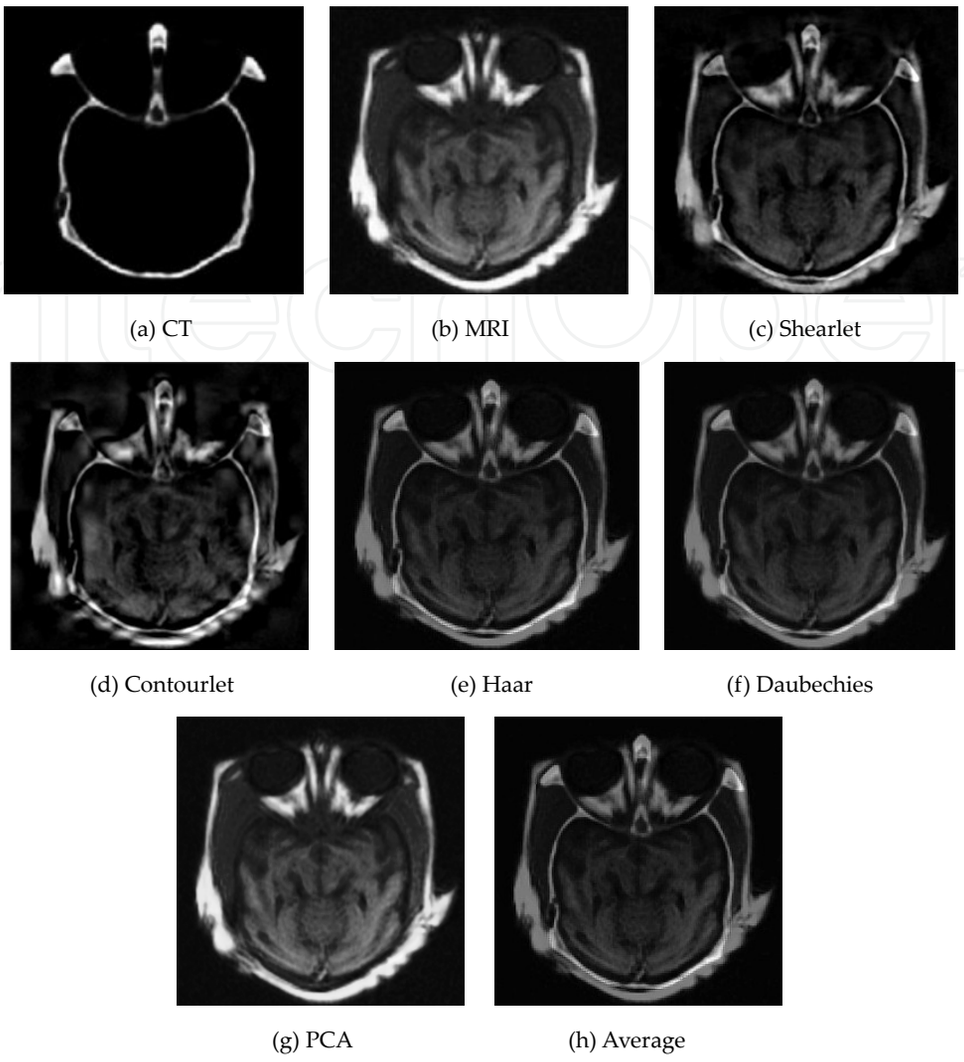

Figure 6. Fusion results on experiment images

4. Remote sensing image fusion based on Shearlets and PCNN

4.1. Theory of PCNN

PCNN, called the third generation artificial neural network, is feedback network formed by the connection of lots of neurons, according to the inspiration of biologic v is ual cortex pattern. Every neuron is made up of three sections: receptive section, modulation and pulse generator section, which can be described by discrete equation [23-25].

The receptive field receives the input from the other neurons or external environment, and transmits them in two channels: F-channel and L -channel. In the modulation on field, add a positive offset on signal L_j from L -channel; use the result to multiply modulation with signal F_j from F-channel. When the neuron threshold $\theta_j \geq U_j$, the pulse generator is turned

off; otherwise, the pulse generator is turned on, and output a pulse. The mathematic model of PCNN is described below [26-30].

$$\begin{cases} F_{ij}[n] = \exp(-\alpha_F)F_{ij}[n-1] + V_F \sum m_{ijkl} Y_{kl}[n-1] + S_{ij} \\ L_{ij}[n] = \exp(-\alpha_L)L_{ij}[n-1] + V_L \sum w_{ijkl} Y_{kl}[n-1] \\ U_{ij}[n] = F_{ij}[n](1 + \beta L_{ij}[n]) \\ Y_{ij}[n] = 1 \quad if\ U_{ij}[n] > \theta_{ij}[n]\ or\ 0\ otherwise \\ \theta_{ij}[n] = \exp(-\alpha_\theta)\theta_{ij}[n-1] + V_\theta Y_{ij}[n-1] \end{cases} \tag{21}$$

Where α_F, α_L is the constant time of decay, α_θ is the threshold constant time of decay, V_θ is the threshold amplitude coefficient, V_F, V_L are the link amplitude coefficients, β is the value of link strength, and m_{ijkl}, w_{ijkl} are the link weight matrix.

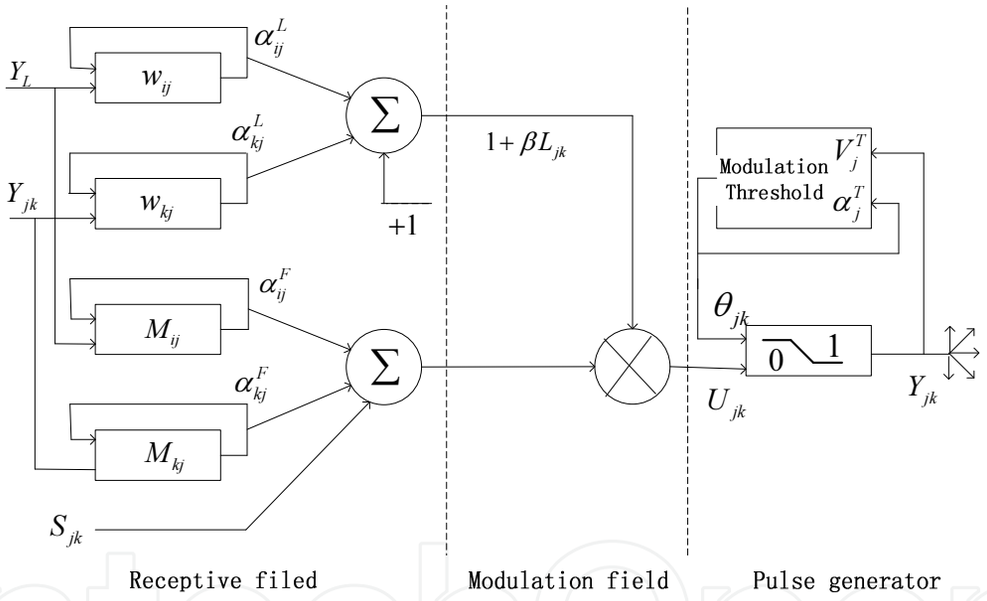

Figure 7. The model of PCNN neuron

4.2. Algorithm framework of remote sensing image fusion using Shearlts and PCNN

When PCNN is used for image processing, it is a single two-dimensional network. The number of the neurons is equal to the number of pixels. There is a one-to-one correspondence between the image pixels and the network neurons.

In this paper, Shearlets and PCNN are used to fuse images. The steps are described below:

1. Decompose the original images A and B respectively into many different directions f_{NA}, $\hat{f}_{NA}$, f_{NB}, $\hat{f}_{NB}$ (N =1, ..., n) via Shear matrixs (In this chapter, n=3).

2. Calculate the gradient features in every direction to form feature maps, $Grad\, f_{NA}$, $Grad\, \hat{f}_{NA}$, $Grad\, f_{NB}$, $Grad\, \hat{f}_{NB}$.

3. Decompose feature map of all directions using DWT, DGf_{NA}, $DG\hat{f}_{NA}$, $DGf_{NB}DG\hat{f}_{NB}$ are high frequency coefficients after the decomposition.

4. Take DGf_{NA}, $DG\hat{f}_{NA}$, $DGf_{NB}DG\hat{f}_{NB}$ into PCNN, and fire maps in all directions $fire\, f_{NA}$, $fire\, \hat{f}_{NA}$, $fire\, f_{NB}$, $fire\, \hat{f}_{NB}$ are obtained.

5. Take the Shearlets on original images A and B, the high frequency coefficients in all directions are f_{NA}^{h}, $\hat{f}_{NA}^{h}$, f_{NB}^{h} and $\hat{f}_{NB}^{h}$, and the low are f_{NA}^{l}, $\hat{f}_{NA}^{l}$, f_{NB}^{l} and $\hat{f}_{NB}^{l}$. The fused high frequency coefficients in all directions can be selected as follow:

$$f_N^h = \begin{cases} f_{NA}^h, & fire\, f_{NA} \geq fire\, f_{NB} \\ f_{NB}^h, & fire\, f_{NA} < fire\, f_{NB} \end{cases}, \qquad \hat{f}_N^h = \begin{cases} \hat{f}_{NA}^h, & fire\, \hat{f}_{NA} \geq fire\, \hat{f}_{NB} \\ \hat{f}_{NB}^h, & fire\, \hat{f}_{NA} < fire\, \hat{f}_{NB} \end{cases}.$$

The fusion rule of the low frequency coefficients in any direction is described below:

$$f_N^l = \begin{cases} f_{NA}^l, & Var\, f_{NA}^l \geq Var\, f_{NB}^l \\ f_{NB}^l, & Var\, f_{NA}^l < Var\, f_{NB}^l \end{cases}, \qquad \hat{f}_N^l = \begin{cases} \hat{f}_{NA}^l, & Var\, \hat{f}_{NA}^l \geq Var\, \hat{f}_{NB}^l \\ \hat{f}_{NB}^l, & Var\, \hat{f}_{NA}^l < Var\, \hat{f}_{NB}^l \end{cases}$$

Where $Varf$ is the variance of f.

6. The fused image is obtained using the inverse Shearlet transform.

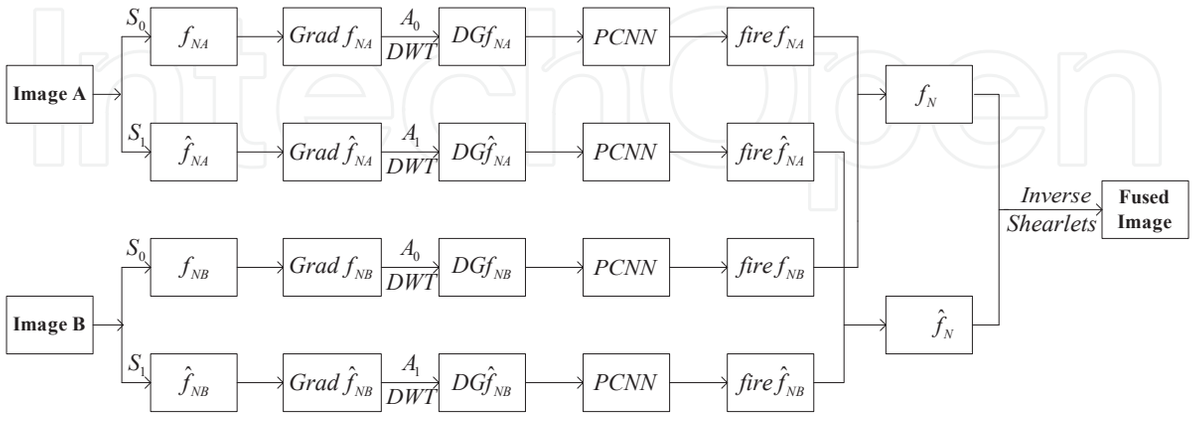

Figure 8. Image fusion framework with Shearlets and PCNN

4.3. Simulation experiments

In this section, three different examples, Optical and SAR images, remote sensing image and hyperspectral image, are provided to demonstrate the effectiveness of the proposed method. Many different methods, including Average, Laplacian Pyramid (LP), Gradient Pyramid (GP), Contrast Pyramid (CP), Contourlet-PCNN (C-P), and Wavelet-PCNN (W-P), are used to compare with our proposed approach. The subjective v is ual perception gives us direct Comparisons, and some objective image quality assessments are also used to evaluate the performance of the proposed approach. The following image quality metrics are used in this paper: Entropy (EN), Overall cross entropy (OCE), Standard deviation (STD), Average gradient (Ave-grad), Q, and $Q_{AB/F}$.

In these three different experiments, the parameters of values of PCNN are showing as follows:

Experiment 1: $\alpha_L = 0.03,\ \alpha_\theta = 0.1,\ V_L = 1,\ V_\theta = 10,\ \beta = 0.2,\ W = \begin{pmatrix} 1/\sqrt{2} & 1 & 1/\sqrt{2} \\ 1 & 1 & 1 \\ 1/\sqrt{2} & 1 & 1/\sqrt{2} \end{pmatrix}$, and the iterative number is $n = 100$.

Experiment 2: $\alpha_L = 0.02,\ \alpha_\theta = 0.05,\ V_L = 1,\ V_\theta = 15,\ \beta = 0.7,\ W = \begin{pmatrix} 1/\sqrt{2} & 1 & 1/\sqrt{2} \\ 1 & 1 & 1 \\ 1/\sqrt{2} & 1 & 1/\sqrt{2} \end{pmatrix}$, and the iterative number is $n = 100$.

Experiment 3: $\alpha_L = 0.03,\ \alpha_\theta = 0.1,\ V_L = 1,\ V_\theta = 15,\ \beta = 0.5,\ W = \begin{pmatrix} 1/\sqrt{2} & 1 & 1/\sqrt{2} \\ 1 & 1 & 1 \\ 1/\sqrt{2} & 1 & 1/\sqrt{2} \end{pmatrix}$, and the iterative number is $n = 100$.

As optical and SAR images, remote sensing image and hyperspectral image are widely used in military, so the study of these images in image fusion are of very important.

Fig.9-11 gives the fused images with Shearlet-PCNN and some other different methods. From Fig.9-11 and Table3, we can see that image fusion based on Shearlets and PCNN can get more information and less distortion than other methods. In experiment 1, the edge feature from Fig. 9(a) and spectral information from Fig. 9(b) are kept in the fused image by using the proposed method, which is showing in Fig.9(c). In Fig.9 (d), the spectral character in the fused image, fused by Contourlet and PCNN, is distorted and the from visual point of view, the color of image is too prominent. From Fig.9 (e)-(f), spectral information of the fused images is lost and the edge features are vague. Fig. 10 are the fused Remote sensing image, which is able to provide more new information since it can penetrate clouds, rain, and even vegetation. With different imaging modalities and different bands, its features are different in each image. In Fig.10(c) and (d), band 8 has more river characteristics but less city information, while band 4 has opposite imaging features.

http://dx.doi.org/10.5772/56945

Fig.10 (c) is the fused image using Shearlets and PCNN. The numerical results in Fig.5 and Table 1 show that the fused image based on Shearlets and PCNN keep better river information, and even involve excellent city features. In Fig 10.(d), in the middle of the fused image using Contourlet and PCNN, has obvious splicing effect. Fig.11(c) is the fused Hyperspectral image. Fig.11(a) and (b) are the two original images, The track of the airport is clear in Fig.11(a), however, some planes information are lost. Fig. 11(b) shows the different information. In the fused image, the track information is more clearly, and aircrafts characters are more obvious. But lines on the runways are not clear enough in the fused images using other methods. From Table 3 we can see that most metric values using the proposed method are better than other methods do.

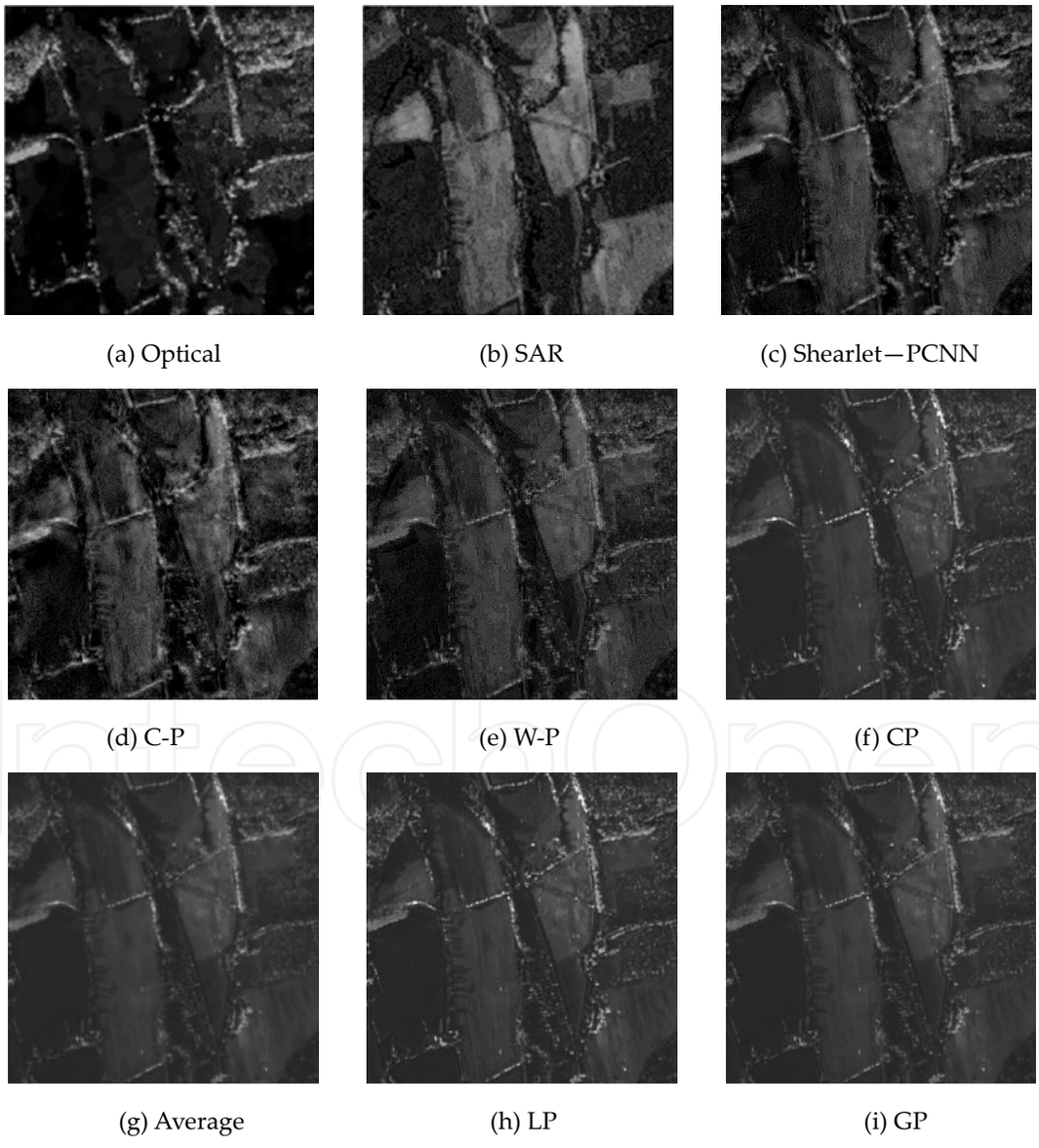

Figure 9. Optical and SAR images fusion results based on Shearlets and PCNN

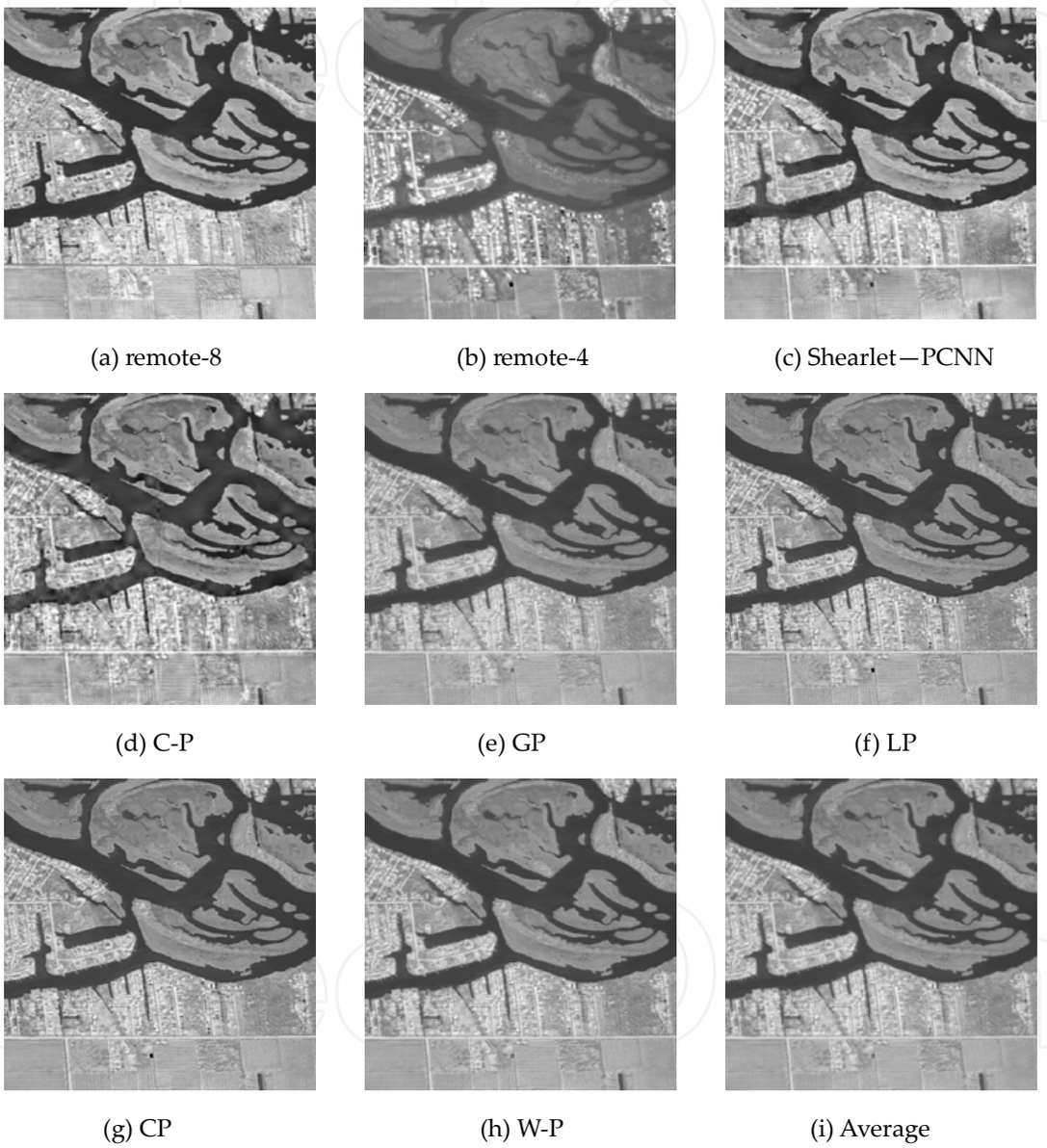

(a) remote-8 (b) remote-4 (c) Shearlet—PCNN

(d) C-P (e) GP (f) LP

(g) CP (h) W-P (i) Average

Figure 10. Remote sensing image fusion results based on Shearlets and PCNN

http://dx.doi.org/10.5772/56945

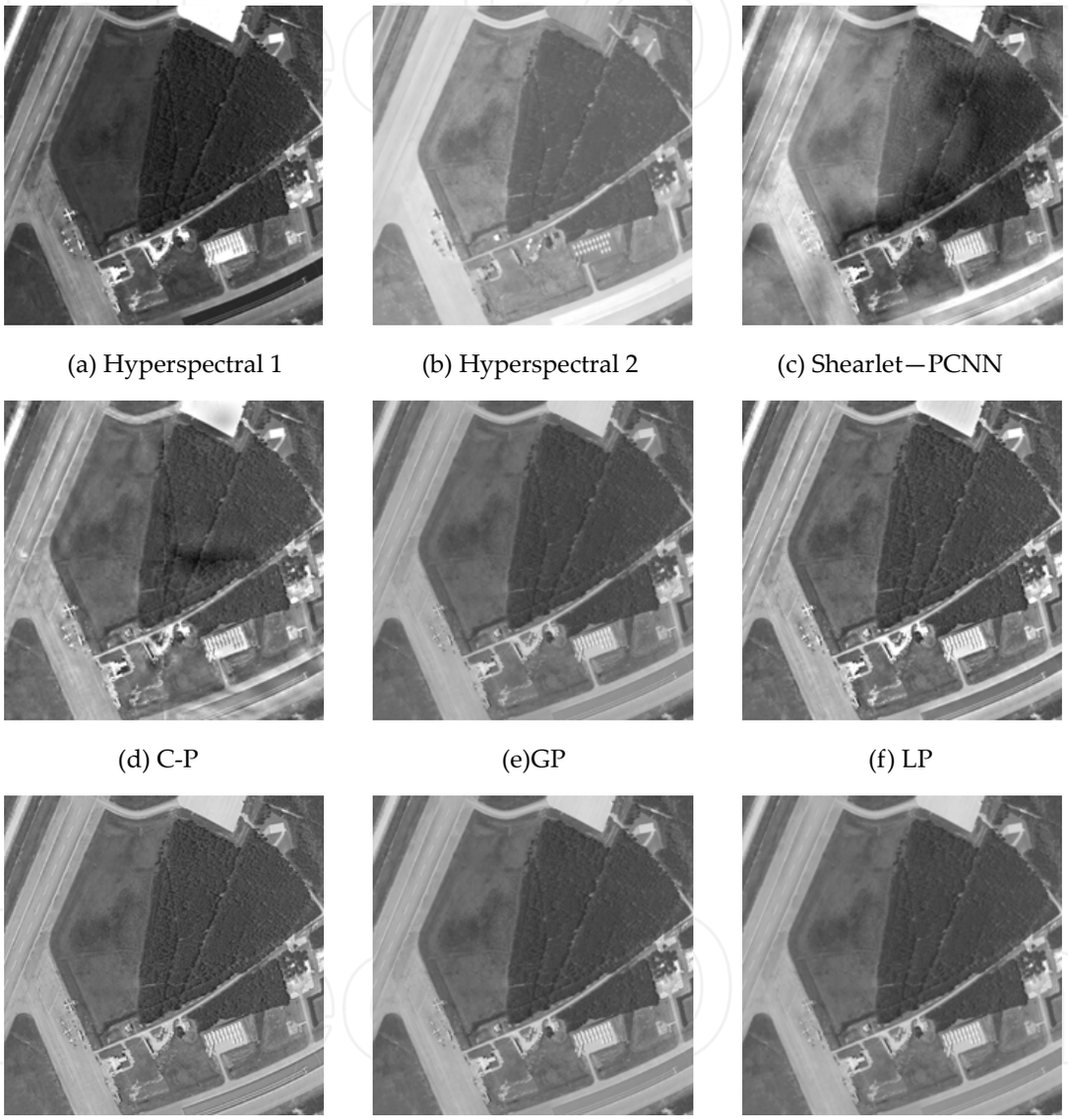

(a) Hyperspectral 1 (b) Hyperspectral 2 (c) Shearlet—PCNN

(d) C-P (e)GP (f) LP

(g) CP (h) W-P (i) Average

Figure 11. Hyperspectral image fusion results based on Shearlets and PCNN

Dataset	Algorithm	$Q_{AB/F}$	Q	EN	STD	Ave-grad	OCE
Experiment 1	Average	0.1842	0.2908	6.3620	22.1091	0.0285	3.2870
	LP	0.3002	0.3017	6.5209	24.8906	0.0478	3.0844
	GP	0.2412	0.2953	6.3993	22.6744	0.0379	3.2336
	CP	0.2816	0.2961	6.4759	24.1864	0.0457	3.1292
	C-P	0.3562	0.4523	6.7424	31.2693	0.0665	0.5538
	W-P	0.3753	0.4976	6.6142	25.2683	0.0662	0.5689
	proposed	0.4226	0.5010	6.9961	34.1192	0.0575	0.5410
Experiment 2	Average	0.4016	0.7581	6.1975	46.1587	0.0236	2.9600
	LP	0.5219	0.7530	6.9594	49.2283	0.0399	3.3738
	GP	0.4736	0.7599	6.9024	47.0888	0.0342	3.6190
	CP	0.5120	0.7475	6.9237	48.9839	0.0392	3.3812
	C-P	0.5658	0.7516	7.3332	54.3504	0.0390	3.0628
	W-P	0.4283	0.7547	6.8543	47.3304	0.0346	3.2436
	proposed	0.6212	0.7775	7.1572	56.2993	0.0381	2.9046
Experiment 3	Average	0.5021	0.7955	6.5011	41.0552	0.0161	1.0939
	LP	0.6414	0.7728	6.8883	47.4990	0.0274	0.9959
	GP	0.5720	0.7898	6.5649	41.3974	0.0223	1.0249
	CP	0.5909	0.7469	6.7499	43.4631	0.0318	0.9834
	C-P	0.5838	0.7435	6.9451	46.5294	0.0262	1.1745
	W-P	0.5319	0.7788	6.5847	41.6623	0.0231	1.5318
	proposed	0.6230	0.7502	7.0791	55.9533	0.0246	0.5246

Table 3. Comparison of image quality metrics

5. Conclusion

The theory of Shearlets is introduced in this chapter. As a novel MGA tool, shearlets offer more advantages over other MGA tools. The main advangtage of shearlets is that it can be studied within the framework of a generalized Multi-Resolution Analysis and with directional subdivision schemes generalizing those of traditional wavelets. This is very relevant for the development of fast algorithmic implementations of the many directional representation systems proved in the last decade.

In this chapter, we have succeed in demonstrations that shearlets are very competitive formulti-focus image and remote sensing image fusion. As a new MGA tool, Shearlet is equipped with a rich mathematical structure similar to wavelet and can capture the information in any direction. And the edge and orientation information are more sensitive than gray according to human visibility. We take full advantage of multidirection of Shearlets and gradient information to fuse image. Moreover, PCNN is selected as a fusion rule to select the fusion coefficients. Because the character is tics of directional and gradient facilitate motivating PCNN neurons, the more precise image fusion results are gotten. Several different kinds

of images, shown in the experiments, prove that the new algorithm we proposed in this chapter is effective.

After development in recent years, the theory of Shearlets is gradually improving. But the time complexity of Shearlets decomposition has been the focus of the study. Which need further study, especially in its theory and applications. We will focus on other image processing methods using shearlets in our future work.

Author details

Miao Qiguang, Shi Cheng and Li Weisheng

References

[1] S. G. Mallat, Theory for Multiresolution Signal Decomposition: The Wavelet Representation, IEEE Transaction on Pattern Analysis and Machine Intelligence, 11(1989),pp: 674-693.

[2] A. Krista, Z.Yun, D.Peter, Wavelet Based Image Fusion Techniques — An introduction, review and comparison, International Society for Photogrammetry and Sensing, 62(2007), pp: 249-263.

[3] J. P. Antoine, P. Carrette, R. Murenzi, B. Piette, Image Analysis with Two Dimensional Continuous Wavelet Transform. Signal Processing, 31(1993), pp: 241-272.

[4] F. G. Meyer, R. R. Coifman, Brushlets: A Tool for Directional Image Analysis and Image Compression. Applied and Computational Hamonic Analysis, 4(1997), pp: 147-187.

[5] N. Kingsbury, Complex Wavelets for Shift Invarian Analysis and Filtering of Signals. Applied and Computational Hamonic Analysis, 10(2001), pp: 234-253.

[6] P. Brémaud , Mathematical principles of signal processing: Fourier and wavelet Analysis, New York, 2002.

[7] Y. Xiao-Hui, J. Licheng, Fusion Algorithm for Remote Sensing Images Based on Nonsubsampled Contourlet Transform, Acta Automatica Sinica,34(2008), pp: 274-281.

[8] E. J. Candes, and D. L. Donoho, Continuous curvelet transform. I. Resolution of the wavefront set, Applied Computational Harmonic Analysis, 19 (2005), pp:162-197.

[9] M.N.Do, M.Vetterli, The Contourlet Transform: An Efficient Directional Multiresolution Image Representation, IEEE Transaction on Image Processing, 14(2005), pp: 2091-2106.

[10] M. QiGuang, W. BaoShu, Multi-Focus Image Fusion Based on Wavelet Transform and Local Energy, Computer Science, 35(2008), pp: 231-235.

[11] Wang-Q Lin, The Discrete Shearlet Transform: A New Directional Transform and Compactly supported Shearlet Frame, 5(2010), pp:1166-1180.

[12] G. Easley, Demetrio Labate and Wang-Q Lim, Sparse Directional Image Representations using the Discrete Shearlet Transform, Applied Computational Harmonic Analysis, 25(2008), pp: 25-46.

[13] G.Kutyniok. and D. Labate, Construction of Regular and Irregular Shearlet Frames, Journal of Wavelet Theory and Applications, 1(2007), pp: 1-10.

[14] G. Kutyniok and Wang-Q Lin, Image Separation Using Wavelets and Shearlets, Lecture Notes in Computer Science, 6920(2012), pp:416-430.

[15] K.Guo and D.Labate, Optimally Sparse Multidimensional Representation using Shearlets, SIAM Journal on Mathematical Analysis, 39(2007), pp: 298-318.

[16] G. Kutyniok and D. Labate, Resolution of the Wavefront Set using Continuous Shearlets, Trans. Amer. Math. Soc, 361(2009), pp:2719-2754. Shearlet webpage, http://www.shearlet.org.

[17] K. Guo, W. Lim, D. Labate, G. Weiss, E. Wilson. The theory of wavelets with composite dilations[J]. Harmonic Analysis and Applications. 4(2006), pp:231–249.

[18] K. Guo, W. Lim, D. Labate, G. Weiss, E. Wilson. Wavelets with composite dilations and their MRA properties[J]. Appl. Comput. Harmon. Anal.,20(2006), pp:231–249.

[19] K. Guo, D. Labate and W. Lim, Edge Analysis and Identification using the Continuous Shearlet Transform, Applied Computational Harmonic Analysis, 27(2009), pp: 24-46.

[20] G. Kutyniok and Wang-Q Lin, Image Separation Using Wavelets and Shearlets, Lecture Notes in Computer Science, 6920(2012), pp:416-430.

[21] K. Guo, W. Lim, D. Labate, G. Weiss, E. Wilson. Wavelets with composite dilations[J]. Electron. Res. Announc. Amer. Math. Soc., 10(2004), pp:78–87.

[22] R. Eckhorn, H. J. Reitboeck, M Arndt et al. Feature linking via synchronization among distributed assemblies: Simulation of results from cat cortex, Neural Computation, 2(1990), pp: 293-307.

[23] R. Eckhorn, H. J. Reitboeck, M Arndt et al. Feature linking via Stimulus-Evoked Oscillstions: Experimental Results form Cat Visual Cortex and Functional Implications form Network Model. In:Proc Int JCNN, Washington D C. 1(1989), pp:723-730.

[24] W. Jin, Z. J. Li, L. S. Wei, H. Zhen, The improvements of BP neural network learning algorithm, Signal Processing Proceedings ,2000, WCCC-ICSP 2000. 5th International Conference on, 3(2000),pp: 1647-1649.

[25] R. P. Broussard, S. K. Rogers, M. E. Oxley et al, Physiologically motivated image fusion for object detection using a pulse coupled neural network , IEEE Trans. Neural Network,10(1999), pp:554-563.

[26] W. Chen, L.C. Jiao, Adaptive tracking for periodically time-varying and nonlinearly parameterized systems using multilayer neural networks, IEEE Trans. on Neural Networks, 21(2010), pp:345-351.

[27] W. Chen, Z.Q. Zhang, Globally stable adaptive backstepping fuzzy control for output-feedback systems with unknown high-frequency gain sign, Fuzzy Sets and Systems, 161(2010), pp: 821-836.

[28] X.B.Qu, J.W.Yan, Image Fusion Algorithm Based on Features Motivated Multi-channel Pulse Coupled Neural Networks, Bioinformatics and Biomedical Engineering, 1(2008),pp: 2103-2106.

[29] X.B.Qu, C.W. Hu, J.W.Yan, Image Fusion Algorithm Based On Orientation Information Motivated Pulse Coupled Neural Networks, Intelligent Control and Automation, 1(2008),pp: 2437-2441.

[30] G.R. Easley, D. Labate, and F. Colonna, Shearlet Based Total Variation Diffusion for Denoising, IEEE Trans. Image Process. 18(2009),pp: 260-268.

IntechOpen